# Cycloid motions of grains in a dust plasma*

Yong-Liang Zhang(张永亮), Fan Feng(冯帆), Fu-Cheng Liu(刘富成),
Li-Fang Dong(董丽芳), and Ya-Feng He(贺亚峰)†

*Hebei Key Laboratory of Optic-electronic Information Materials, College of Physics Science and Technology, Hebei University, Baoding* 071002, *China*

(Received 21 August 2015; revised manuscript received 23 October 2015; published online 10 January 2016)

Hypocycloid and epicycloid motions of irregular grains (pine pollen) are observed for the first time in a dust plasma in a two-dimensional (2D) horizontal plane. These cycloid motions can be regarded as a combination of a primary circle and a secondary circle. An inverse Magnus force originating from the spin of the irregular grain gives rise to the primary circle. Radial confinement resulting from the electrostatic force and the ion drag force, together with inverse Magnus force, plays an important role in the formation of the secondary circle. In addition, the cyclotron radius is seen to change periodically during the cycloid motion. Force analysis and comparison experiments have shown that the cycloid motions are distinctive features of an irregular grain immersed in a plasma.

**Keywords:** dust plasma, irregular grain, cycloid motions

**PACS:** 52.27.Lw, 52.40.Kh, 52.90.+z **DOI:** 10.1088/1674-1056/25/2/025201

## 1. Introduction

The dust plasma is characterized by charged grains immersed in a plasma of electrons and ions.[1–3] The grains could acquire charges of the order of $10^3$ to $10^4$ elementary charges and often become strongly coupled, which gives rise to novel phenomena such as the crystallization, phase transitions, and waves.[4–9] The grains suspended in sheath suffer gravitation force, electrostatic force, drag force, and sometime external magnetic/laser field etc. It leads to complex motions of grains like gyromotion, cluster rotation and shear flow.[10–17] It is obvious that a charged grain could perform gyromotion if it is magnetized in external magnetic field. The measurements of gyroradius and cyclotron frequency provide an effective method for the noninvasive determination of the charge on a grain.

Most of studies on the dust plasma either in experiment or in theory deal with grain of a spherical form, such as the glass, melamine formaldehyde, and alumina mocrosphere.[3–5] In some cases, especially in the numerical simulation of molecular dynamics, for simplicity, the grain is considered as a charged particle neglecting the grain shape. However, the grains appeared in planetary rings, fusion reactors, materials processing, etc., generally have a nonspherical shape. The dynamics of the nonspherical grain in the dust plasma is less known at present.

A grain immersed in a plasma suffers the momenta transferred from plasma flux and surrounding gas.[1–3] This could result in the spin of the grain and has been paid much attention in recent years.[18–20] For an ideal spherical grain, the net effect for the momenta transfer can be zero. For a grain with irregular shape the net transfer of the angular momenta can be estimated as $\eta_{\rm ass}\pi a^2 n_{\rm i,\infty} m_{\rm i} a v_s v_\infty$[18] (where $\eta_{\rm ass}$ is the coefficient taking into account the degree of irregularity of the dust shape, $a$ is the average radius of the grain, $n_{\rm i,\infty}$ is the ion density, $m_{\rm i}$ is the ion mass, $v_{\rm s}$ is the ion velocity at the surface of the grain when they are attached to the grain and $v_\infty$ is the ion velocity far from the grain). The angular frequency of such spin can reach a rather large value ($\sim 10^4$ s$^{-1}$–$10^9$ s$^{-1}$).[19] The spin of a hollow glass microsphere with defect has been detected with angular velocity up to 12000 rad/s in a stratified glow discharge.[19] The spin of a charged grain could give rise to a magnetic moment. Interacting with external magnetic field, the spinning grain is subjected to a magnetic force which could result in the complex motions of such grain.[18,21] However, in the absent of external magnetic field, a spinning grain could also exhibit complex motions which have not been well studied until now. Here, we report an experimental study on the cycloid motions of irregular grains (pine pollen) in a dusty plasma. Hypocycloid and epicycloid motions are observed, besides the stationary grain and the circle motion of grain. The inverse Magnus force originated from the spin of the grain is considered, and it plays important role on the cycloid motions of grains. These complex motions of grains are explained based on the force analysis in 2D horizontal plane. Additional comparison experiments with regular microspheres are performed in order to confirmed that the cycloid motions are distinctive features of a pine pollen immersed in a plasma.

*Project supported by the National Natural Science Foundation of China (Grant Nos. 11205044 and 11405042), the Natural Science Foundation of Hebei Province, China (Grant Nos. A2011201006 and A2012201015), the Research Foundation of Education Bureau of Hebei Province, China (Grant No. Y2012009), the Program for Young Principal Investigators of Hebei Province, and the Midwest Universities Comprehensive Strength Promotion Project.

†Corresponding author. E-mail: Heyf@hbu.edu.cn

© 2016 Chinese Physical Society and IOP Publishing Ltd 

## 2. Experimental setup

Figure 1 shows the sketch of the experimental apparatus. The experiments are carried out in a vacuum chamber with a background pressure within $p = 10$–$70$ Pa. Argon gas at flow of 10 sccm is used for the discharge. In order to avoid disturbances in grain motion during an experiment the position of the gas inlet is designed properly. Plasma is produced by coupling capacitively the electrode to a radio-frequency generator (13.56 MHz). The forward power varies from 5 W to 50 W. The separation between the lower stainless steel electrode and the upper ITO coated electrode is 70 mm. Due to the lack of probe, the plasma parameters are obtained by using numerical simulations with a two-dimensional fluid model based on the continuity equations for mass, momentum and electron energy, and Poisson equation for the electric field.[22] The electron density is $n_e = 1.8 \times 10^{10}$ cm$^{-3}$ and the electron temperature is $T_e = 2.2$ eV under the given experimental conditions, which are in agreement with the experimental results by Basner.[23]

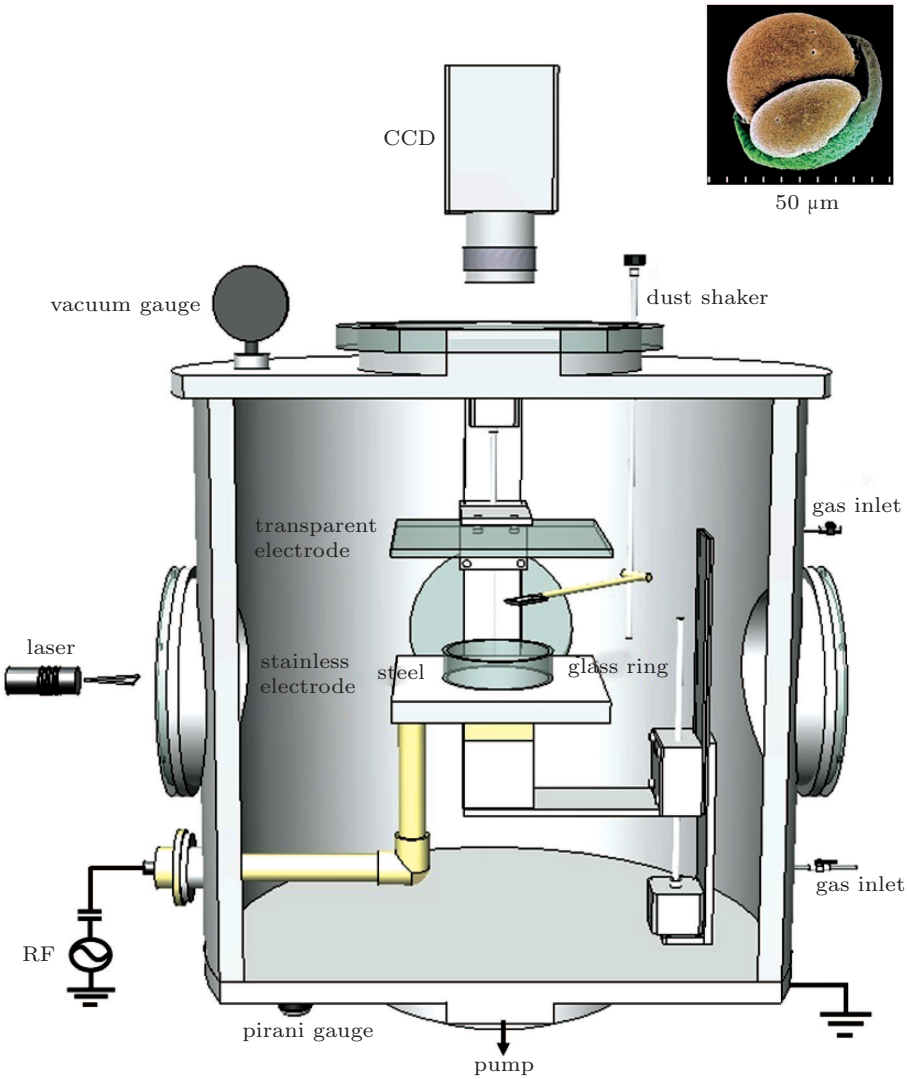



**Fig. 1.** (color online) Schematic diagram of the experimental setup. The inset shows the image of a pine pollen we used in experiments.

Pine pollen having nonspherical shape as shown by the inset in Fig. 1 are injected into the plasma through a shaker and serve as dust grains. The average radius is about $(20 \pm 5)$ μm. The charge $Q$ of a dust grain can be obtained by means of the methods of force balance and/or resonance frequency,[24] $Q \simeq 5 \times 10^4 e$. One or few grains are injected into the plasma during each experiment in order to avoid the formation of grain ring and plasma condensation. Regular glass and resin microspheres are also used in comparison experiments. Grain is horizontally illuminated by a 50-mW, 532-nm laser sheet with a thickness of 0.5 mm and imaged by a CCD camera from the upper transparent electrode. The spatial and temporal resolutions are 10 μm/pixel and 50 frames/s, respectively. The trajectory of grain can be obtained by using long-time exposure. In order to obtain the velocity and acceleration of grain a high speed camera (PCO.dimax, 1000 fps) is used. Characteristic parameters of the grain movement are measured by using the image processing with MATLAB.

A glass ring is positioned on the lower stainless steel electrode. The diameter and the height of the glass ring are 37 mm and 10 mm, respectively. After being injected into the plasma, charged grain levitates nearby the glass wall. Due to the circular symmetry of the glass ring the grain travels around the glass ring or stays near its equilibrium position.

## 3. Experimental results

### 3.1. Regular movements of grains

We firstly show the regular movement of a single grain around the glass ring in a 2D horizontal plane as shown in Fig. 2. Figure 2(a) shows an epicycloid motion with inward petals. This meandering motion can be regarded as a combination of two circular motions, where the primary circle (radius $r_2$) orbits the secondary circle (radius $r_1$) in one direction with angular velocity $\omega_1$ and spins about its center in the same direction with angular velocity $\omega_2$ as shown by the diagram of Fig. 3(a). Figure 2(c) shows a hypocycloid motion with outward petals with rotations in the opposite sense [as illustrated by the diagram of Fig. 3(b)]. The epicycloid and hypocycloid motions occur in two cases, respectively. The epicycloid trajectory is observed only outside of the glass ring, and the value of angular velocity satisfies $\omega_1\omega_2 > 0$. The hypocycloid trajectory is found both inside and outside the glass ring, and the value of angular velocity satisfies $\omega_1\omega_2 < 0$. For the two kinds of cycloid motions they both satisfy the following relation:

$$|r_1\omega_1| < |r_2\omega_2|, \tag{1}$$

i.e., the linear speed of the secondary circle is less than that of the primary circle. This is a key to the formations of the petals on both epicycloid and hypocycloid trajectories.

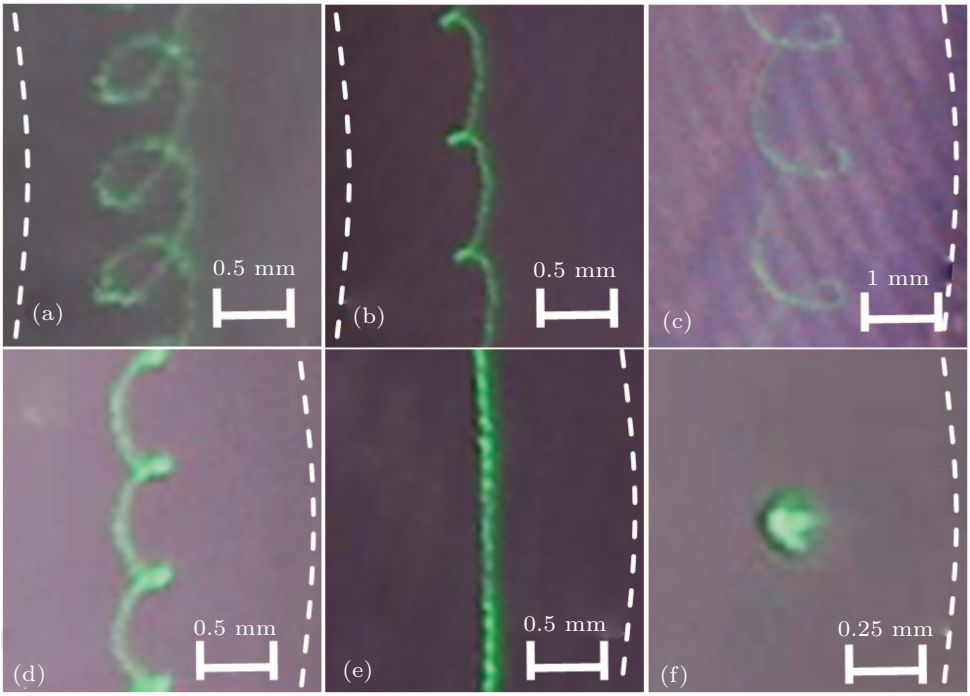



**Fig. 2.** (color online) Trajectories of travelling (a)–(e) and stationary (f) grains. Dashed line in each image indicates schematically the glass ring. Panels (a) and (b) are located outside the glass ring. Panels (c)–(f) are located inside the glass ring. (a): epicycloid motion; (b): cuspate epicycloid motion; (c): hypocycloid motion; (d): cuspate hypocycloid motion; (e): circular motion; (f): stationary grain. Exposure times of panels (a)–(f) are: 0.39, 0.26, 0.53, 0.16, 0.32, 1 s, respectively.

Cuspate epicycloid and hypocycloid motions are observed as shown in Fig. 2(b) and 2(d), respectively. In these cases, the radius $r_{1,2}$ and the angular velocity $\omega_{1,2}$ follow the condition:

$$|r_1\omega_1| \geq |r_2\omega_2|. \tag{2}$$

This means that the linear speed of the secondary circle is equal or greater than that of the primary circle, which leads to the appearance of the cusps on the cuspate cycloid trajectories. The cuspate epicycloid motion is observed only outside the glass ring, and the value of angular velocity satisfies $\omega_1\omega_2 > 0$. The cuspate hypocycloid motion is observed both inside and outside the glass ring, and the value of angular velocity satisfies $\omega_1\omega_2 < 0$.

Circular motion is observed both inside and outside the glass ring as shown in Fig. 2(e). The angular speed of circular motion of grain changes within the range of 0.05 rad/s–1.23 rad/s. Stationary grain is observed both inside and outside the glass ring as shown in Fig. 2(f). In the absent of action with other grain, the grain is considerably stable at higher gas pressure. However, Brownian motion of grain is observed clearly

at lower gas pressure. The grain moves stochastically near its equilibrium position. This has also been reported by other groups.[25]

Which trajectory a grain will follow is determined by the initial conditions (such as the initial position and the angular velocity) of the dropped grain and the discharge parameters. This means that for several grains dropped simultaneously (or one grain dropped repeatedly), they (it) will exhibit different trajectories because their (its) initial conditions are not exactly the same. Therefore, the dependencies of the parameters $r_{1,2}$ and $\omega_{1,2}$ mentioned above on the gas pressure and the forward power of discharge could not be illustrated evidently. In our experiments, the radii of the primary and the secondary circles change within the ranges of $r_2 = 0.08$ mm–0.57 mm and $r_1 = 13$ mm–25 mm, respectively. The corresponding values of angular velocities change within the ranges of $\omega_2 = 24$ rad/s–88 rad/s and $\omega_1 = 0.03$ rad/s–0.63 rad/s, respectively.

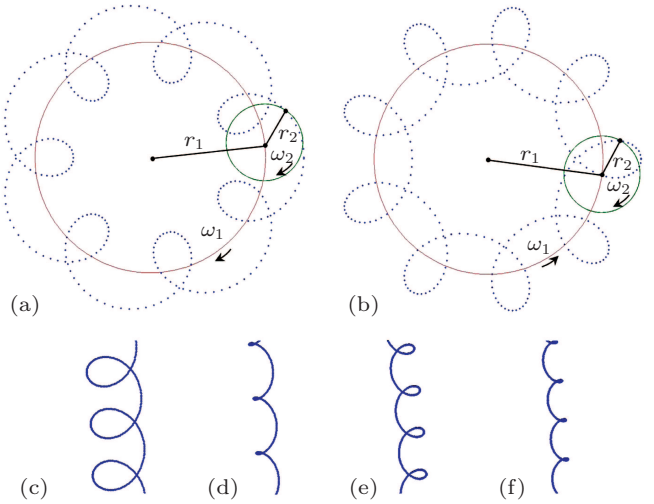



**Fig. 3.** (color online) Schematic diagram of cycloid motions. (a): epicycloid; (b): hypocycloid. Dotted line represents the trajectory of cycloid motions of grains. Solid line and dashed line indicate the primary circle and the secondary circle, respectively. $r_2$ and $r_1$ represent the radii of the primary and the secondary circles, respectively. $\omega_2$ and $\omega_1$ represent the angular velocities of the primary and the secondary circles, respectively. Panels (a) and (b) occur when $\omega_1\omega_2 > 0$ and $\omega_1\omega_2 < 0$, respectively. Panels (c)–(f) reproduce the trajectories as shown in Figs. 2(a)–2(d) in term of Eqs. (1)–(4). The parameters are $\omega_1 = 0.14$, 0.15, 0.42, 0.22 rad/s, $\omega_2 = 44.52$, 27.45, $-45.13$, $-32.63$ rad/s, $r_1 = 20.39$, 20.27, 12.31, 13.17 mm, $r_2 = 0.21$, 0.14, 0.25, 0.12 mm in Figs. 2(a)–2(d) and Figs. 3(c)–3(f), respectively.

The (cuspate) cycloid motions of grains follow the parameter equations in polar coordinate if we pick the center of glass ring as the origin:

$$r^2 = r_1^2 + r_2^2 + 2r_1 r_2 \cos(\omega_2 - \omega_1)t, \tag{3}$$

$$\theta = \omega_1 t \pm \arccos\left(\frac{r_1 + r_2\cos(\omega_2 - \omega_1)t}{r}\right), \tag{4}$$

where, "+" and "−" correspond the cases of $\sin(\omega_2 - \omega_1)t > 0$ and $\sin(\omega_2 - \omega_1)t \leq 0$, respectively. $r$ and $\theta$ represent the radial and azimuth positions of grains in polar coordinate, respectively. $\omega_i$ and $r_i$ $(i = 1, 2)$ are defined as above. By using the measured $\omega_1$, $\omega_2$, $r_1$, $r_2$ in Fig. 2(a)–2(d), we can reproduce the observed cycloid motions in term of Eqs. (1)–(4) as shown in Fig. 3(c)–3(f). Due to the pressure on the grain from the horizontal laser, there are some distortions on the experimental cycloid trajectories [Fig. 2(a)–2(d)] as compared with Fig. 3(c)–3(f).

### 3.2. Force analysis

The force analysis for a nonspherical grain, like the pine pollen we used, becomes very complex. These forces mainly include the gravitation force, electrostatic force, ion drag force, neutral friction force, and inverse Magnus force. The inverse Magnus force, which originates from the spin of a nonspherical grain, is considered here for the first time. The interaction force between grains is not considered in the present case because only one or few grains separated well are dropped in each experiment.

The gravitation force $F_g = mg$ acts downward vertically and will not be considered here because our emphases is on the horizontal motions of dust grains.

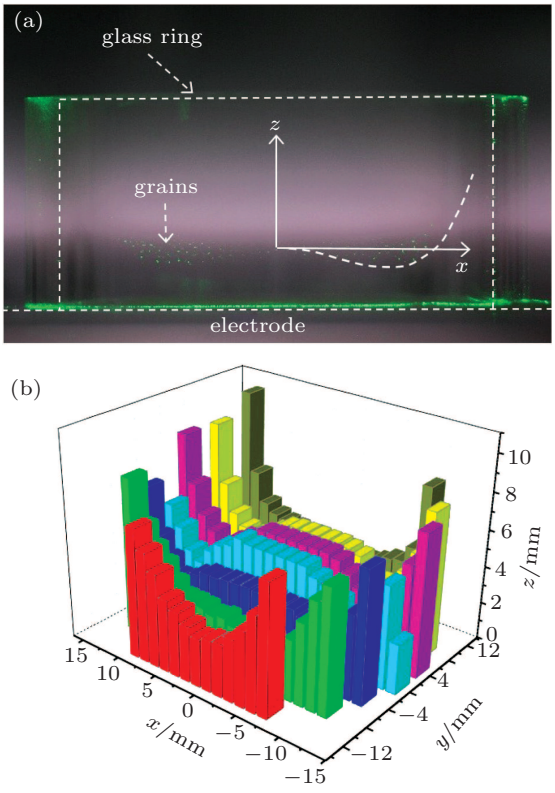



**Fig. 4.** (color online) Sheath profile indicated by the grain distribution in $x$–$z$ plane at $y = 0$ mm (a) and in three-dimensional (3D) space (b). Radial profile of the sheath inside the glass ring is indicated by the dropped grains illuminated by a vertical laser sheet. Gas pressure is 15 Pa and forward power is 8 W.

The electrostatic force originates from the action of sheath field on the negatively-charged grain. In the present of a glass ring the sheath profile follows approximately the walls of the glass ring and the electrode. Because the thickness of sheath near the glass ring and the electrode are different,[26]

the confinement of the sheath to the grain becomes complex. When the diameter of the glass ring is small, the horizontal confinement to the grain could be described by a parabolic potential, and the grain is confined to the center of the glass ring.[3] Here, the glass ring is relatively large, and the grain is restricted near the glass wall both inside and outside. In order to obtain the radial distribution of the sheath, we drop plenty of grains into the glass ring and capture the grain distribution in $x$–$z$ plane illuminated by a vertical laser sheet as shown in Fig. 4(a). The sheath profile inside the glass ring can be obtained approximatively by fitting the bottom profile of grain distribution by superposing 20 images as indicated by the dashed line in Fig. 4(a). If we pick the center of glass ring as the origin of polar coordinate, the radially confining potential is fitted approximately by a quartic polynomial:

$$U(r) = 0.0005r^4 - 0.038r^2, \tag{5}$$

here, $r$ represents the radial distance to the center of the glass ring. For the sake of simplicity, the radial confinement outside the glass ring has a mirror symmetry about the glass wall as shown by the solid lines in Fig. 6(a). Furthermore, by means of a measurement of spatial resolution in y direction, we can obtain the 3D sheath profile as shown in Fig. 4(b). It can be seen that the sheath near the glass wall is lower than that in the center of the glass ring, which gives rise to the confining potential to the grain. Beyond the minima of the confining potential as indicated by the dashed line in Fig. 6(a), the grain is attracted toward the center of the glass ring. On the contrary, within the minima of the confining potential, the grain is repulsed toward the glass wall. The present of the potential well plays important role to the formation of the cycloid motions of grains.

Ion drag force acting on the grain by ion flow results mainly from Coulomb drag and collection drag, and has been explored extensively. Together with the neutral drag and the plasma charging flux, the ion drag could give rise to the spin of the immersed grain. The spin of a hollow transparent glass microsphere with surface defect was observed in a stratified glow discharge by Karasev *et al.*[19] The values of angular velocity measured in their experiments are between 0 and 12000 rad/s. As a rule, for the nonspherical grain as we used here, the pine pollen would spin faster than the glass microsphere they used because the surface of pine pollen is much irregular than that of glass microsphere. The rapid spin of the pine pollen around its center of inertia gives rise to the inverse Magnus force which plays important role on the complex motions of grains.

The inverse Magnus force results from the spin of a travelling grain in rarefied fluid as illustrated by Fig. 5. As is well known, the normal Magnus force usually occurs in dense fluid (the Knudsen number $Kn = \lambda/d$ is negligibly small, here, $\lambda$ is the mean free path of the fluid, $d$ is the diameter of the grain) and can be described by using the Navier–Stokes equations,[27] which has depicted well the arc trajectory of "banana kick". However, in rarefied fluid (for $Kn \gg 1$), the inverse Magnus force occurs and can be described in term of the method of free molecular flow[28]

$$\boldsymbol{F}_{\rm MI} = -k\eta d^3 \boldsymbol{\omega}_0 \times \boldsymbol{v}, \tag{6}$$

here, $\boldsymbol{\omega}_0$ and $\boldsymbol{v}$ represent the vectors of angular velocity and travelling velocity of a spinning grain, respectively. $\eta$ is the density of fluid. $k$ is a coefficient related with the shape of the grain. The minus sign in Eq. (6) represents the inverse Magnus effect. In our experiment, the mean free path of neutral gas is $\lambda \sim 0.7$ mm ($P = 10$ Pa), the diameter of grain is $d \sim 40$ μm, and the Knudsen number is $Kn \gg 1$. Therefore, the description of fluid dynamical limit is not applicable in this case. Because the inverse Magnus force acts perpendicularly to the travelling direction of the grain, it could provide the centripetal force for the cycloid motion of the grain travelling along the primary circle. Here, we focus on the case that the vector of angular velocity of the spinning grain is along the vertical direction, i.e., the inverse Magnus force acting on the grain is always along the horizontal plane.

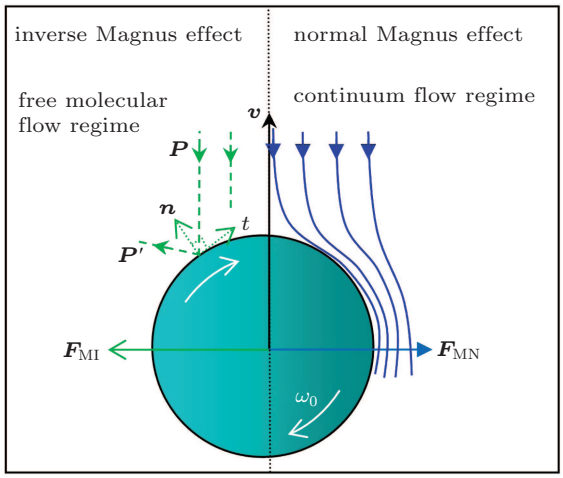



**Fig. 5.** (color online) Schematic diagram of the inverse (normal) Magnus force $\boldsymbol{F}_{\rm MI}$ ($\boldsymbol{F}_{\rm MN}$) acting on a spinning grain. In the free molecular flow regime, $\boldsymbol{P}$ ($\boldsymbol{P}'$) represents the pre-impact momentum (deflected momentum).

The neutral drag force is a resistance force caused by the collisions with the neutral gas molecules. It damps the motion of grain. Therefore a driving force is necessary for the grain to keep moving forward along the orbit. Although the origin of this unknown driving force is still unclear at present, we can give some suggestions. 1) It should be related with the irregularity of the grain, because our comparison experiments with glass and resin microspheres have shown that no cycloid motion and no circle motion are observed. Several groups also reported the rotation of nonspherical agglomerate of microspheres. The rotation of microsphere is observed only

in a magnetized dust plasma, which is induced by the Lorentz force.[6,13] 2) This driving force is nondirectional with regard to the glass ring because both clockwise and counterclockwise rotations are observed. 3) It should be the same order of magnitude of the neutral drag force because the grain could continue to move uniformly along the glass ring. In the following we will neglect the counteractive neutral drag force and driving force.

### 3.3. Origin of the primary circle

The cycloid motion of the grain is characteristic of a combination of the primary and the secondary circles. Therefore, the essential origins of the primary and the secondary circles are keys to understand the formations of these cycloid motions.

For a charged grain travelling along the primary circle in a plasma, a persistently centripetal force is required. As is well known, the Lorentz force and the inverse Magnus force are characteristic of their transverse action with respect to the travelling direction of an object. However, no magnetic field is applied to the charged grain in our experiments. Therefore, only the inverse Magnus force appears and provides the persistently centripetal force for the rotation of the grain along the primary circle. Other forces mentioned above cannot provide persistently centripetal action on the travelling grain. For example the horizontal components of the electrostatic force and ion drag force act only in radial direction due to the rotational symmetry of the glass ring. Although those forces are not the origin of the primary circle, they play important role in the formation of the secondary circle.

The spin of the irregular charged grain is the key to the cycloid motion via inverse Magnus effect. In order to confirm these distinctive features of the cycloid motions the pine pollen has exhibited as shown above, further experiments with glass and resin microspheres are performed at the same discharge conditions for comparison (not shown here). No cycloid motion is observed. Those regular microspheres (less spin) show behaviours such as the random motion and the crystallization as other groups observed previously. Therefore, we can draw a conclusion that the spin of the pine pollen gives rise to the inverse Magnus force which provides the centripetal force for the primary circle.

### 3.4. Origin of the secondary circle

Our observations of the cycloid motions of grains can be classified roughly into four groups (I)–(IV) as shown by the diagrams in Fig. 6(b). The equilibrium line $L$ indicates the position of minimum of the radially confining potential.

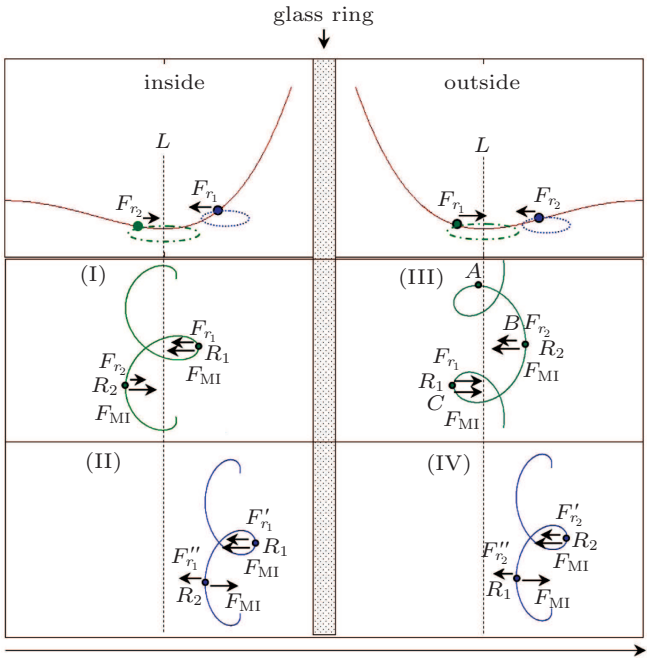



**Fig. 6.** (color online) Schematic diagram of the grain trajectories. Solid lines in panel (a) illustrate the approximate profile of sheath in vertical section. Equilibrium line $L$ (dashed line) indicates the position of the minima value of confining potential. $F_1$ represents the horizontal component of the radially confining force when the grain is between the equilibrium line $L$ and the glass wall. Outside this region, it is expressed as $F_2$. Panel (b) shows four cases of complex trajectories in a horizontal plane. (I), (II), and (IV) show the hypocycloid motions, and (III) shows the epicycloid motion. $F_{\rm MI}$ represents the inverse Magnus force. $R_1$ ($R_2$) is the cyclotron radius when the grain is near (far away from) the glass wall.

For the case (III), the grain meanders near the equilibrium line $L$. The centripetal forces at points $B$ and $C$ read:

$$F_{{\rm c}_C} = F_{\rm MI} + F_{r_1} = \frac{mv^2}{R_1}, \tag{7}$$

$$F_{{\rm c}_B} = F_{\rm MI} + F_{r_2} = \frac{mv^2}{R_2}. \tag{8}$$

Here, $F_{r_1}$ is slightly larger than $F_{r_2}$ due to the steep sheath near the glass wall, therefore the cyclotron radii $R_1 < R_2$. The periodical change of the cyclotron radius as the grain travelling gives rise to the epicycloid trajectory as illustrated by Fig. 2(a).

The centripetal force $F_{\rm c}$ consists of inverse Magnus force $F_{\rm MI}$ and radial confinement force $F_{\rm r}$ as shown by Eqs. (7) and (8). $F_{\rm c} = mv^2/r$ and $F_{\rm r} = ma_{\rm r}$ can be obtained experimentally from the grain trajectory with high speed camera at the frame of 1000 fps. Figure 7(a) shows the dependance of the centripetal force $F_{\rm c}$ on the time within two cycles. It can be seen that the centripetal force at point $C$ (case III in Fig. 6) is $F_{{\rm c}_C} = 3.4 \times 10^{-11}$ N, the centripetal force at point $B$ is $F_{{\rm c}_B}$=$2.7 \times 10^{-11}$ N, $F_{{\rm c}_C} > F_{{\rm c}_B}$. Obviously, the magnitude of radially confining forces $F_{\rm r}$ at points $B$ and $C$ are in accord with $F_{\rm c}$ as shown in Fig. 7(b), i.e., $|F_{{\rm r}_C}| > |F_{{\rm r}_B}|$. Near the equilibrium line $L$, as indicated by point A in Fig. 6(b) III, the radial confinement disappears, $F_{\rm r} = 0$, as shown in Fig. 7(b). In this case, only inverse Magnus force plays the role of centripetal force, i.e., $F_{{\rm c}A} = F_{\rm MI}$. Therefore, we can obtain the

inverse Magnus force $F_{\rm MI} = F_{cA} = 1.44 \times 10^{-11}$ N. In Eq. (6), $\eta \sim 9 \times 10^{-4}$ kg/m$^3$ at 50 Pa, $d \sim 40$ μm, and $v \sim 0.04$ m/s obtained from the trajectory, then we have $k\omega_0 \simeq m\omega_2/\eta d^3 \simeq 5 \times 10^6$ rad/s. Here, if we suppose $k \simeq 5\pi$ for the pine pollen, which is five times than that for a microsphere, the value of the angular velocity of spin is about $\omega_0 \simeq 3 \times 10^5$ rad/s. This value is reasonably larger than that observed by Karasev *et al.* ($1.2 \times 10^4$ rad/s) because the pine pollen we used is more irregular than the hollow transparent glass microsphere they used. However, experimental detection of such a grain spinning faster is out of the reach of our camera at present.

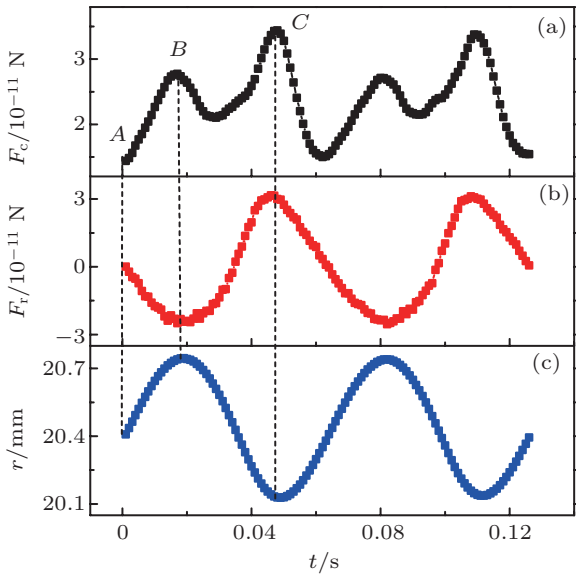



**Fig. 7.** (color online) Dependance of the centripetal force $F_{\rm c} = mv^2/r$ (a), the radially confining force $F_{\rm r} = ma_{\rm r}$ ($m$: grain mass, $a_{\rm r}$: radial acceleration) (b), and the radial position $r$ (c) of grain on time. These measured results correspond to the grain outside the ring which follows the epicycloid trajectory as shown by Fig. 2(a) and Fig. 6(b) III. The origin of polar coordinate is set to the center of the glass ring. The capitals *A*–*C* correspond to those in Fig. 6(b) III. The magnitudes of $F_{\rm c}$ and $F_{\rm r}$ at point *B* is smaller than that at point *C*.

The above force analysis is also applicable to the case (I). However, because the small cyclotron radius $R_1$ is located outside the equilibrium line $L$ in case (I), the periodical change of the cyclotron radius results in the hypocycloid trajectory as illustrated by Fig. 2(c). Particularly, if the grain is more closer to the glass wall, $F_{r_1}$ becomes stronger, the petals would turn into cusps, which results in the formation of cuspate hypocycloid trajectory as illustrated by Fig. 2(d).

For the case (II), the grain meanders between the equilibrium line $L$ and the glass wall. The centripetal forces near and far away from the glass wall are:

$$F_{\rm c1} = F_{\rm MI} + F'_{r_1} = \frac{mv^2}{R_1}, \tag{9}$$

$$F_{\rm c2} = F_{\rm MI} - F''_{r_1} = \frac{mv^2}{R_2}. \tag{10}$$

Obviously, the cyclotron radii $R_1 < R_2$. The cyclotron radius changes periodically as the grain travelling, which results in the hypocycloid motion. The above analysis is also applicable to the case (IV). In addition, if we assume $F'_{r_1} \simeq F'_{r_2}$ due to the small radius $r_2$ of the primary circle and add Eq. (9) and Eq. (10) together, then we have $F_{\rm MI} \simeq (F_{c1} + F_{c2})/2$. From the measured $F_{\rm c1}$ and $F_{\rm c2}$ we can obtain that $F_{\rm MI}$ is of the order of $10^{-11}$ N.

## 4. Conclusions and remarks

In this work, we have studied the cycloid motions of irregular grains (pine pollen) in a dusty plasma in a 2D horizontal plane. Hypocycloid motions are observed both inside and outside the glass ring. Epicycloid motion is observed only outside the glass ring. The radially confining potential from the sheath is experimentally measured, which play important role in the formation of cycloid motions of grains. Based on the force analysis and the measured trajectories of grain with high speed camera, the inverse Magnus force is obtained to be of the order of $10^{-11}$ N, and the value of the angular velocity is of the order of $10^5$ rad/s. The observed cycloid motions of grains result from the periodical change of the cyclotron radius near and far from the glass wall. Additional comparison experiments with regular microspheres are performed in order to confirmed that the cycloid motions are distinctive features of a pine pollen immersed in a plasma.

Recently, some studies focused on the Magnus effect in optical manipulation,[29] in a Bose–Einstein condensate,[30] and in lattice models of superfluids.[31] They have revealed that the Magnus force is larger than that predicted by theoretical models and allows one to perform particle trapping. Our results have also revealed that the Magnus effect an irregular grain exhibited in plasma environment can not be negligible and would play important role on the complex motions of the grains. It is also suggested that these complex motions of irregular grains we observed could be found in fusion reactors because the grown or sputtered grain could have considerable angular speed of spin.

In addition, the vector of angular velocity of a spinning grain is not limited to the vertical direction as we discussed above. Due to the stochastic initial conditions of a dropped grain, this vector could point at other directions in three dimensional space. This means that the inverse Magnus force acting on a spinning grain could point out of the horizontal plane. Therefore, the inverse Magnus force together with the other forces will give rise to more complex motions of grains in three dimensional space. This will be the subject of a future study.

## References

[1] Morfill G E and Ivlev A V 2009 *Rev. Mod. Phys.* **81** 1353
[2] Fortov V E, Khrapak A G, Khrapak S A, Molotkov V I and Petrov O F 2004 *Phys. Usp.* **47** 447

[3] Shukla P K and Eliasson B 2009 *Rev. Mod. Phys.* **81** 25
[4] Chu J H and Lin I 1994 *Phys. Rev. Lett.* **72** 4009
[5] Zhdanov S K, Nosenko V, Thomas H M, Morfill G E and Couëdel L 2014 *Phys. Rev. E* **89** 023103
[6] Hou L J, Wang Y N and Miskovic Z L 2005 *Phys. Plasmas* **12** 042104
[7] Huang F, Ye M F and Wang L 2004 *Chin. Sci. Bull.* **49** 2150
[8] Wu Jing, Zhang P Y, Sun J Z, Zhang J, Ding Z F and Wang D Z 2008 *Chin. Phys. B* **17** 1848
[9] Bonitz M, Henning C and Block D 2010 *Rep. Prog. Phys.* **73** 066501
[10] Ott T, Löwen H and Bonitz M 2014 *Phys. Rev. E* **89** 013105
[11] Feng Y, Liu B and Goree J 2008 *Phys. Rev. E* **78** 026415
[12] Liu D Y, Wang D Z and Liu J Y 2000 *Acta Phys. Sin.* **49** 1094 (in Chinese)
[13] Carstensen J, Greiner F, Hou L J, Maurer H and Piel A 2009 *Phys. Plasmas* **16** 013702
[14] Saitou Y and Ishihara O 2013 *Phys. Rev. Lett.* **111** 185003
[15] Wang X G, Wang Z X, Wang C H and Guo B 2002 *Phys. Plasmas* **9** 4396
[16] Zou X, Liu J Y, Wang Z X, Gong Y, Liu Y and Wang X G 2004 *Acta Phys. Sin.* **53** 3409 (in Chinese)
[17] Baruah S and Das N 2010 *Phys. Plasmas* **17** 073702
[18] Tsytovich V N, Sato N and Morfill G E 2003 *New J. Phys.* **5** 43
[19] Karasev V Yu, Dzlieva E S, Eikhvald A I, Ermolenko M A, Golubev M S and Ivanov A Yu 2009 *Phys. Rev. E* **79** 026406
[20] Hutchinson I H 2004 *New J. Phys.* **6** 43
[21] Schwabe M, Konopka U, Bandyopadhyay P and Morfill G E 2011 *Phys. Rev. Lett.* **106** 215004
[22] Liu F C, He Y F and Dong L F 2014 *Phys. Plasmas* **21** 123503
[23] Basner R, Sigeneger F, Loffhagen D, Schubert G, Fehske H and Kersten H 2009 *New J. Phys.* **11** 013041
[24] Melzer A, Trottenberg T and Piel A 1994 *Phys. Lett. A* **191** 301
[25] Schwabe M, Zhdanov S, Rath C, Graves D B, Thomas H M and Morfill G E 2014 *Phys. Rev. Lett.* **112** 115002
[26] Schubert G, Haass M, Trottenberg T, Fehske H and Kersten H 2012 *Contrib. Plasma Phys.* **52** 827
[27] Borg K I, Söderholm L H and Essén H 2003 *Phys. Fluids* **15** 736
[28] Weidman P D and Herczynski A 2004 *Phys. Fluids* **16** L9
[29] Cipparrone G, Hernandez R J, Pagliusi P and Provenzano C 2011 *Phys. Rev. A* **84** 015802
[30] Turner A M 2009 *Phys. Rev. Lett.* **103** 080603
[31] Sonin E B 2013 *Phys. Rev. B* **88** 214513